Time-resolved temperature measurements during pulsed laser irradiation using thin film metal thermometers

D. P. Brunco
Department of Materials Science and Engineering, Cornell University, Ithaca, New York 14853

J. A. Kittl
Division of Applied Sciences, Harvard University, Cambridge, Massachusetts 02138

C. E. Otis
IBM T. J. Watson Research Center, Yorktown Heights, New York 10598

P. M. Goodwin
Mail Stop M888, Los Alamos National Laboratory, Los Alamos, New Mexico 87545

Michael O. Thompson
Department of Materials Science and Engineering, Cornell University, Ithaca, New York 14853

M. J. Aziz
Division of Applied Sciences, Harvard University, Cambridge, Massachusetts 02138

In this article, we describe a technique using NiSi and Pt thin film metal thermometers to provide accurate temperature information on a nanosecond time scale during pulsed laser processing of materials. A surface layer of interest is deposited onto the thermometer layer, and temperatures are determined from temperature dependent changes in the metal film's resistance. Details concerning the design and fabrication of the device structure and experimental considerations in making nanosecond resolved resistance measurements are discussed. Simple analytical estimates are presented to extract quantities such as incident laser energy stored in the sample. Finally, transient temperature data in the thermometer film, in combination with heat flow calculations, allow temperature determination as a function of time and depth into the sample and, additionally, can provide information about material properties of the surface layer.

I. INTRODUCTION

Pulsed laser irradiation of materials is extensively used for rapid heating and cooling of surface layers with minimal temperature rises in the bulk. Temperature gradients resulting from short pulse irradiation produce extremely rapid cooling of the surface via thermal conduction into the bulk, with peak cooling rates in excess of 10^{11} K/s. Some of the more widely studied systems include pulsed laser melting of Si, laser-induced quenches of metallic glasses, and pulsed laser ablation of polymer and ceramic materials.[1]

Pulsed laser melting of silicon ($T_{melt} = 1687$ K) illustrates the range of temperatures readily accessed with lasers. A 30 ns, 1.0 J/cm^2 XeCl laser (308 nm) pulse will create a surface liquid in Si to a depth of about 200 nm. Within 100 ns, the surface will have solidified; a microsecond later, the surface temperature will have fallen to below 700 K. A similar XeCl laser pulse, at a fluence of 80 mJ/cm^2, incident on polyimide, will heat the surface to ≈ 1700 K, leading to thermal decomposition and etching. Nanosecond resolved temperature measurements over such large temperature ranges and shallow depths are essentially impossible using conventional temperature sensing devices such as thermocouples and pyrometers. Consequently, one normally must estimate temperatures from numerical heat flow simulations. However, these calculations are often compromised by poor knowledge of specific heats, thermal conductivities and optical properties at the temperatures of interest. Polymer ablation provides a good example since these properties cannot be measured at temperatures even approaching 1700 K. Additionally, the materials properties of thin films may differ substantially from those obtained in bulk measurements, further compromising temperature estimates obtained from simulations.

Limitations in numerical modeling and a need for firm experimental temperature data have led to a number of time-resolved techniques for extracting temperatures. In 1982, Larson et al.[2] studied ruby laser irradiated silicon using nanosecond resolved x-ray diffraction. Measured heat-induced lattice expansion was related to temperature using the Si thermal expansion coefficient. Temperatures in silicon were also estimated by Compaan[3] using time-resolved Raman spectroscopy as a probe. More recently, optical transmission measurements in laser irradiated amorphous silicon on quartz[4] have been combined with calculations to provide temperature data. In addition to silicon based systems, temperatures in metallic and polymeric systems have also been pursued. Herman and Elsayed-Ali,[5] using time-resolved reflection high energy electron diffraction (RHEED), measured superheatings of up to 120 K prior to melting of Pb(111) surfaces. Laser ablation threshold temperatures in poly-(methyl methacrylate) (PMMA) have recently been measured with a novel "molecular thermometer" technique.[6] The PMMA is doped with a dye having a temperature dependent absorp-

tion coefficient and optical transmission is used to probe temperature.

While these techniques provide useful temperature data for the particular system they are designed to measure, the applicability of these techniques to other systems is often limited. For example, the x-ray experiments require a synchrotron source and are limited to single crystal materials. Measurements based upon optical transmission require transparent substrates and either a material with a significant temperature dependent absorption or one that can be doped with a dye having such properties. The RHEED technique is limited to single crystals and must be performed in ultrahigh vacuum with clean crystal surfaces. Also, requirements on experimental apparatus are extensive.[5]

In this paper, we provide fabrication and analysis details on a technique for transient temperature measurements of the near surface region during pulsed laser irradiation. This technique is capable of making subnanosecond resolved temperature measurements over a range in excess of 1000 K with absolute accuracies of ±20 K and relative accuracies of 1 K. These temperature measurements are obtained by monitoring the transient resistance of a thin metal film fabricated below an absorbing layer. Temperatures within the structure can then be inferred by coupling the direct temperature measurements at a known depth in the sample with one-dimensional heat flow simulations. Temperature extrapolations from this combined experimental/numerical process are quite accurate since values near the region of interest are measured directly.

The use of a surface thin film thermometer to measure temperatures during nanosecond laser irradiation was first described by Thompson in 1988.[7] That initial work used a semiconductor layer (Si) for the thermometer to provide high sensitivity over a limited range. Subsequent applications have used metallic thermometers (NiSi and Pt) over the full range from room temperature to the melting point of Si.[8-11] Most recently, the temperature reached during pulsed laser ablation of polyimide was measured using NiSi thermometers,[9,10] and the congruent melting temperatures of Si:As alloys were measured using Pt thermometers.[11] The technique, though, is quite general and by suitable choice of materials can be applied to a wide range of problems.

II. DESIGN OF EXPERIMENT

A. Sample design

In their simplest form, samples consist of a thin metal film fabricated on an insulating substrate, with the material to be irradiated deposited on the surface (Fig. 1). An isolation layer, e.g., SiO_2 or Si_3N_4, may be necessary between the thermometer and surface layers to electrically isolate the thermometer and/or avoid chemical interactions between these layers. Incident laser radiation is absorbed by the surface layer with subsequent heat conduction through the thermometer material and into the substrate. As the thermometer temperature rises, its electrical resistance in-
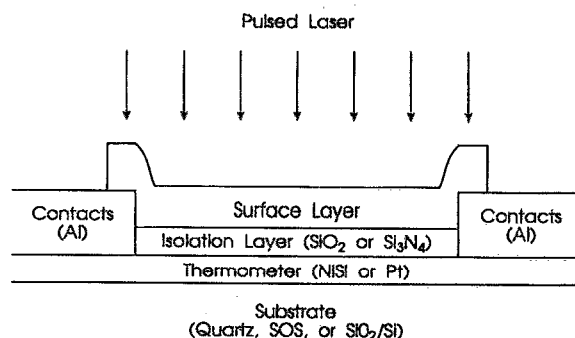

FIG. 1. Schematic of the basic sample design. For electrically conducting surface layers, the design must be slightly modified to avoid shorting the Al contacts.

creases. This temperature dependent resistance can be calibrated by quasi-static furnace measurements prior, or subsequent, to laser irradiation. Hence, from time-resolved resistance measurements on the metal film, a direct measure of the temperature at (or near) the lower boundary of the surface layer is made. A number of practical issues, however, must be considered in the design of the actual sample structure. Several of the more important issues involved, including selection of materials for the thermometer, surface layer, and substrate, as well as device geometry and dimensions, are discussed below.

1. Thermometer materials

The ideal thermometer should minimally perturb the system under measurement while reporting temperatures as close as possible to the region of interest. In the sample structure, this requires that the thermometer layer be thermally thin compared to other layers in the system. This is necessary both to ensure nearly uniform temperatures within the thermometer and to present a negligible perturbation to overall heat flow in the system. Although thermally thick thermometers can be quantitatively handled in heat flow simulations, there are significant advantages to working in the thermally thin regime. First, the minimal thermal load of a thin thermometer allows for measured temperatures that are higher and closer to actual temperatures achieved in the surface layer. Secondly, since the accuracy of heat flow calculations are limited by the quality of materials parameters used as inputs, thinner thermometer layers minimize errors by minimizing the effects of uncertainty in thermometer materials properties. The lower limit on thicknesses is determined by film uniformity, physical damage thresholds, and the requirement that thermometers have resistances of approximately 100 Ω for maximum sensitivity (Sec. II B).

The thermometer material must satisfy several requirements itself. The material should have low resistivity to permit use of thin layers with the desired 100 Ω resistance, should have a high thermal conductivity to minimize temperature gradients across the thermometer, should be easy to fabricate reproducibly, and should be relatively unreactive to adjacent layers in the sample structure. In practice, the electrical and thermal conductivity requirements are

coupled for metals by the Wiedemann-Franz law; good electrical conductors are necessarily good thermal conductors. Additionally, the resistance versus temperature characteristic should be linear, or near linear, over the temperature range of interest with a large temperature coefficient of resistance ($\gamma = 1/R \, dR/dT$). For elemental metals with low residual resistances, the coefficient of resistivity at room temperature can approach 0.0034 K^{-1} ($\approx 1/T$). However, γ is typically reduced due to finite grain size and alloy effects.

Since electrical properties of thin films often differ from bulk values and may additionally show a significant dependence upon processing conditions, calibrations of resistance versus temperature on actual devices are crucial. These calibrations are generally carried out in a static furnace environment with the temperature ramped at relatively slow rates. Ideally, such calibrations behave linearly over the full temperature range of interest. However, the linear range observable in slow-ramping furnace calibrations is sometimes limited by irreversible changes in thermometer microstructure (annealing) or degradation from interactions with neighboring layers. In contrast, the rapid heating and quenching associated with laser processes typically allow insufficient time for annealing or thermal degradation, even at temperatures substantially above the linear regime found in furnace calibrations. In these cases, the low temperature behavior during furnace calibrations may be extrapolated to higher temperatures. This extrapolation introduces additional uncertainty and hence materials and structures that allow calibration over the widest possible temperature range are preferred.

Finally, thermometer materials must be robust since devices are often required to withstand relatively high transient powers and temperatures. The Si:As on Pt thermometer structure to be described in Sec. III B is a good example. For 30 ns laser irradiation at the modest fluence of 0.5 J/cm^2, the peak incident power reaches a value of 33 MW/cm^2, and a maximum Pt temperature of over 1000 K is reached in under 100 ns.[11]

Two materials, Pt and NiSi, have been successfully used by our groups for temperature measurements. Both exhibit linear temperature dependent resistivities with reasonable γ values and are easily processed using traditional microelectronic processing techniques. Although NiSi was initially used because of its simpler processing, Pt is now preferred because of the higher calibration temperatures possible.

2. Surface layers

This temperature measurement technique is primarily applicable to surface materials which are either strongly absorbing to the incident laser irradiation, or moderately absorbing with high thermal conductivities. Since the thermometer monitors the temperature near the bottom of the surface layer, extrapolation of temperatures to the surface are more accurate for thin surface layers. To avoid direct heating of the thermometer by laser radiation, however, the surface must be optically thick (at least 3 absorption depths). This constraint is generally satisfied by most ma-

terials of interest in laser processing; weak absorbers do not show good laser processing characteristics and are of limited interest at present. As an example, Si under UV irradiation has an absorption coefficient of $\sim 1 \times 10^6$ cm^{-1} and requires surface layers at least 30 nm thick. For polymers with absorption coefficients near 10^5 cm^{-1}, minimum film thicknesses must be on the order of 300 nm.

Optical opacity of the surface layer is one concern; the thermal transparency is another. Materials with high thermal conductivities have small thermal gradients and thus minimal differences between the surface temperature and the measured temperature at the back interface. If a surface material of interest is neither a strong absorber nor a good thermal conductor, thin surface layers may be used if the laser absorption and reflection from the sample structure is included in numerical modeling. This process requires accurate knowledge of the optical properties of the surface film, as well as of the thermometer and boundary layers.

Finally, the surface material should be well-characterized thermally (conductivity and specific heat) and optically (absorption coefficient and reflectivity) if heat flow simulations are required to extract temperatures in the surface layer. Poorly known thermal and/or optical properties may be measured, to a degree, from experiments performed on several different and accurately known thicknesses of the absorbing material. Comparison of the measured time-resolved temperatures with numerically determined temperatures provide a consistency check on the estimated materials properties used in calculations.

3. Substrate

The substrate choice is largely determined by the application, e.g., high thermal conductivity substrates to form metallic glasses or for rapid solidification studies.[11] However, substrates with low thermal conductivities increase the peak magnitude of the temperature transient and substantially simplify the temperature analysis. For a given incident fluence, the temperature rise in the thermometer scales roughly with $1/\sqrt{\rho c \kappa}$, where ρ, c, and κ are the density, specific heat, and thermal conductivity of the substrate [see Eq. (4.1)]. Among the three substrates used in our studies, silicon, quartz, and silicon-on-sapphire (SOS), quartz wafers offers a $1/\sqrt{\rho c \kappa}$ ratio about 7 times more favorable than that for SOS and 10 times that for Si. In practice, the magnitude of the peak temperatures observed do not scale precisely with $1/\sqrt{\rho c \kappa}$ since other factors contribute to heat flow in the overall sample structure. Additionally, low thermal conductivity substrates are slower in removing heat from the near surface region, providing additional time for measurements. Finally, it is beneficial if the substrate is available in wafer form for microfabrication.

In addition to the attributes desirable for each individual layer, it is advantageous that all materials have reasonably well-known thermal properties and the surface layer be well-characterized optically. As will be discussed in Sec. IV C, heat flow simulations provide a powerful tool for
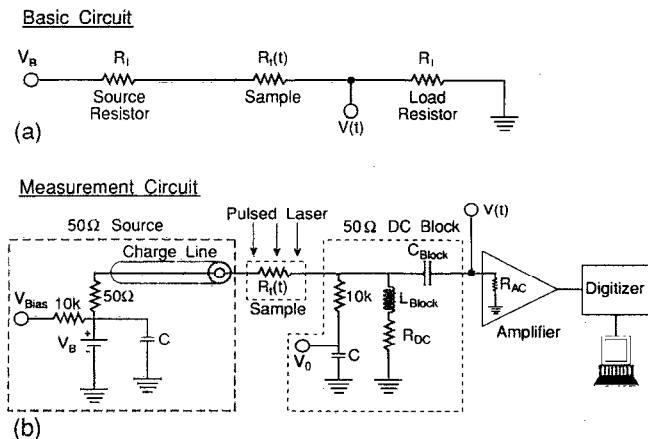
Basic Circuit

(a)

Measurement Circuit

(b)

FIG. 2. Diagram of simplified (a) and actual (b) circuit used to obtain time-resolved resistance measurements. R_{ac} and R_{dc} are nominally 50 Ω. C_{block} is ≈ 12 μF and L_{block} is ≈ 20 mH, though exact values are not critical.

analysis of thermometer temperature profiles but their accuracy is limited by the quality of the input materials parameters.

4. Patterning

As mentioned earlier, thermometers should be patterned for resistances of approximately 100 Ω for maximum sensitivity. Assuming a resistivity of 25 $\mu\Omega$ cm for a 50 nm Pt film, the length to width aspect ratio for the thermometer should be approximately 20. The absolute dimensions may be scaled arbitrarily with two caveats. First, the laser irradiation must be uniform over the total dimensions of the device. Second, linewidths must be sufficiently wide to ensure nominal 1D heat flow, i.e., much wider than the thermal diffusion length $\sqrt{4Dt}$, where D is the thermal diffusivity of the substrate and t is the maximum time of interest. For quartz wafers and a time of 10 μs, this implies a linewidth greater than 6 μm. Device lines are typically made much wider (50–100 μm) to simplify fabrication and ensure sample uniformity. Typically, photolithographic masks are used with 50 to 100 μm linewidths and a total device active area confined within a 1×1 mm square. A meandering path can be used to define a large aspect ratio resistor using reasonable linewidths and still remaining within a 1 mm^2 active area. Large pads, overcoated with a few hundred nm of Al, provide for electrical contact to the measuring circuit.

B. Time-resolved temperature measurements

Since temperature measurements on nanosecond time scales are desired, it is necessary to measure the time-dependent resistance of the thermometer with bandwidths in excess of 300 MHz. Conventional resistance measurements based on constant voltage or current sources are unable to respond at these speeds and hence a transmission line configuration is employed.[12] The basic configuration is diagrammed in Fig. 2 (a). In concept, the thermometer acts as a coupling resistor between two impedance matched transmission lines (commonly 50 Ω). The input line is

biased by a terminated voltage source V_B. Current is partially reflected and transmitted by the thermometer, with the reflected component terminated in the source. The transmitted current terminates in a load resistor, generating a voltage proportional to the current. For frequencies below roughly c/l, where c is the speed of light and l is a characteristic length of the thermometer, the thermometer can be treated as a lumped component with a simple resistance $R_t(t)$. For typical device dimensions of < 1 cm total length, the bandwidth capability of the samples is > 10 GHz. If R_I is the impedance of the transmission lines (and nominally of the terminating resistors), and $V(t)$ is the time dependent voltage across the terminating load resistor, then

$$R_t(t) = R_I \left[\frac{V_B}{V(t)} - 2 \right]. \tag{2.1}$$

In practice, R_I is 50 Ω and the transmitted current is terminated into either an oscilloscope's 50 Ω vertical amplifier or an equivalent circuit. This provides a convenient means both to properly terminate the transmission line and to measure the voltage. While theoretically the input transmission line need only connect the source bias to the thermometer, a 15 m charge line is normally used to relax the requirements of the voltage source. During laser heating, the current through the sample changes rapidly ($dI/dt \approx 10^3$ A/s). Rather than design the source to respond at this rate, a long charge line (length $= L$) is used to isolate the source and thermometer in time, $\Delta t \cong 2L/c$. Dispersion in the charge line reduces the dI/dt and relaxes source bias requirements. These considerations are important primarily for very high speed measurements in excess of 50 MHz. With the use of a charge line, the bias source can be a simple power supply, a series of fast capacitors to provide the transient current, and a 50 Ω carbon film resistor (wire wound precision resistors cannot be used because of a large inductive resistance at the frequencies of interest). Since power supplies do not normally respond in submicrosecond time scales, a hierarchy of capacitors from 0.001 μF ceramic disks (fast transient response) to 10 μF tantalum (slow response) are used to provide the constant voltage over the time frame of the measurement. A 10 μF capacitor will limit the voltage droop over 100 μs to less than 10% even if the dc voltage supply were disconnected.

From the resistance measurement, the temperature can be estimated using a linear relationship between resistance and temperature, $R_t(T) = R_0[1 + \gamma(T - T_0)]$, where R_0 is the resistance at temperature T_0 and γ is the temperature coefficient of resistivity. From this linear relation, the time dependent temperature can be estimated from the measured voltage by

$$T(t) = T_0 + \frac{1}{\gamma} \left[\left(\frac{V_B/V(t) - 2}{V_B/V_0 - 2} \right) - 1 \right], \tag{2.2}$$

where V_0 is the observed voltage at T_0. The sensitivity, $|dV/dT|$, of the devices to small changes in temperature (near T_0) is given by

$$\left|\frac{dV}{dT}\right| = \gamma V_B \left[\frac{R_0/R_I}{(2+R_0/R_I)^2}\right]. \tag{2.3}$$

The maximum sensitivity of $\gamma V_B/8$ occurs for a thermometer resistance equal to twice the impedance ($R_0/R_I = 2$). This maximum is fairly broad, however, so that devices with room temperature resistances between 50 and 200 Ω yield sensitivities within 10% of the maximum. For a typical temperature coefficient of resistivity of 0.001 K^{-1} and a 1 V bias, the sensitivity is approximately 125 μV/K on a background voltage V_0 of 250 mV.

The small temperature dependent signal is superimposed on a large dc bias as described above. Consequently, our measurement system separately records the dc and ac components of the signal; the complete measurement circuit is shown in Fig. 2(b). For the dc component of the signal, the current is shunted through the inductor L_{block} and a resistor to ground. The resistor is chosen such that the total dc resistance of the inductor and resistor equals 50 Ω. On time scales short compared to L_{block}/R_{dc}, the inductor current remains fixed at the dc value. Wire resistances limit L_{block} to approximately 20 mH, giving a maximum time for measurements of 40 μs at 10% droop. A 10 kΩ tap resistor and capacitor to a dc voltmeter provides the static dc voltage measurement V_0. The ac signals are shunted through C_{block} to a wide-band 50 Ω amplifier or oscilloscope; the 12 μF capacitor provides a low frequency cutoff of approximately 250 Hz. The ac signal is digitized and stored for subsequent computer analysis. (Note: 50 Ω ac scope inputs are usually 50 Ω to ac but blocking to dc. This is not universal, however. The output of the diagrammed circuit may be fed directly to the dc 50 Ω input.)

In the derivation of Eq. (2.2), the source and terminating resistors were taken as equal to the transmission line impedance R_I. This equation can be generalized for times $t < L_{block}/R_{dc}$ in the more complex circuit. Allowing for small differences in the ac and dc impedances (R_{ac} and R_{dc}), Eq. (2) becomes

$$T(t) = T_0 + \frac{1}{\gamma}\left\{\frac{1}{R_0}\left[\frac{V_B - [V_0 + V(t)]}{(V_0/R_{dc}) + (V(t)/R_{ac})} - R_I\right] - 1\right\}. \tag{2.4}$$

Finally, the dc bias current can cause substantial Joule heating of the sample which must be considered. The power delivered into the thermometer,

$$P = \frac{V_B^2}{R_I}\left[\frac{R_0/R_I}{(2+R_0/R_I)^2}\right], \tag{2.5}$$

unfortunately has the same dependence on R_0/R_I as the sensitivity equation. Hence, at maximum sensitivity, sample heating is also maximized. However, since sensitivity scales linearly with V_B while power scales quadratically, the optimal design still requires a sample resistance near $2R_I$. The heating effect can be substantial; a 5 V bias and a 1 mm^2 sample area must dissipate 6.25 W/cm^2. For a well heat sunk Si substrate, the temperature rise is negligible, but is ≈ 20 K for a quartz substrate. For a thermally isolated quartz substrate, the heating rate would be ~ 75 K/s. To avoid such heating effects, bias voltages below 2 V
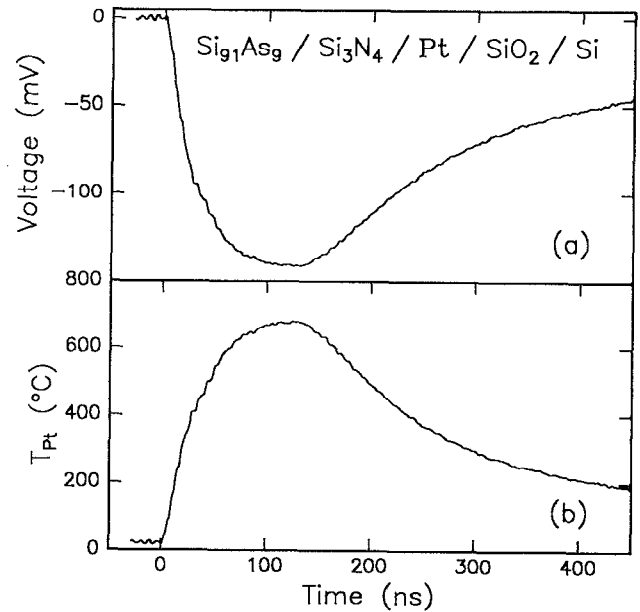

FIG. 3. The ac voltage (a) and Pt temperature (b) vs time for a Si$_{91}$As$_9$ alloy on the Pt thermometer structure.

may be necessary with electronic amplification of the ac signal, or higher bias voltages can be used if applied as a pulse 10 ms prior to the laser transient (sufficient to stabilize the inductor current and precharge the blocking capacitor).

Temperature measurements were made on Pt thermometers with a Si:As surface layer and irradiated using a 308 nm excimer laser. A typical voltage versus time transient is shown in Fig. 3(a), with the conversion from voltage to temperature shown in Fig. 3(b). Experimental conditions for this device were a bias of 2 V, a static resistance of 106 Ω, and a γ of 0.0012 K^{-1}.

III. THERMOMETER FABRICATION AND CALIBRATION

Thermometers were fabricated using conventional photolithographic and microelectronic processing techniques. A schematic of a fabricated device is shown in Fig. 1. The processing of NiSi thermometers on both quartz and silicon-on-sapphire (SOS) wafers and of Pt thermometers on thermally oxidized silicon wafers are described in this section. Devices are relatively simple and a single 75 mm wafer typically yields hundreds of nearly identical devices. The details of fabrication and the device characteristics that result from the indicated processing conditions are presented. Although a few of the processing details discussed are particular to the specific experiment performed, most of the steps concern fabrication in general. Additionally, problems encountered and overcome in these specific studies illustrate some of the broader issues.

A. NiSi thermometers

NiSi thermometers were fabricated on quartz substrates to measure the threshold temperature for laser ablation of polyimide.[9] In a single pumpdown, first silicon

and then nickel were electron beam evaporated at a deposition pressure of 1×10^{-6} Torr onto a quartz wafer and patterned by liftoff into serpentine resistors. The thermometers had a linewidth of 80 μm, a length to width ratio of 65, and a device active area of 1×1 mm^2. The Ni and Si were subsequently reacted to form a silicide by annealing in high vacuum at 275 °C for 80 min and 450 °C for 60 min. The thermometers, as measured by Rutherford backscattering, were 140 nm thick and contained a two phase mixture of predominately NiSi with a small amount of Ni$_2$Si. Because bare NiSi in contact with polyimide corroded during the polyimide curing cycle, a 50 nm layer of SiO$_x$ was deposited over the silicide by plasma enhanced chemical vapor deposition (PECVD) as a corrosion barrier. The oxide was selectively etched with buffered oxide etch (BOE) to allow electrical contact to the thermometer leads. The same masking level was used for self-aligned liftoff patterning of 300 nm thick aluminum contacts to the thermometers. The final device structures exhibited room temperature resistances of typically 240 Ω ($\rho \approx 50\ \mu\Omega$ cm) and temperature coefficients of resistivity of 0.0011 K^{-1}. Once the thermometer structures were complete, polyimide precursors were vapor deposited[13] onto the devices and cured to form PMDA-ODA polyimide layers 100 and 200 nm thick.

Similar devices were also fabricated on SOS substrates. An SOS wafer (nominally 500 nm Si layer) was RCA cleaned and a 40 nm Ni film was thermally evaporated at a pressure of 2×10^{-5} Torr. The devices were photolithographically patterned using the same masks as above. The nickel was etched with Transene nichrome etch[14] and the silicon was reactively ion etched down to the sapphire substrate using an SF$_6$/O$_2$ plasma. A 50 nm PECVD oxide was deposited and patterned, followed by deposition and etching of 300 nm aluminum contacts. Silicidation to form NiSi was accomplished by a two stage vacuum anneal of 250 °C for 30 mins followed by 60 mins at 450 °C. Final devices exhibited resistances of about 125 Ω ($\rho \approx 16$ $\mu\Omega$ cm) and γ's of 0.0040 K^{-1}.

The NiSi thermometers constructed on SOS wafers were of significantly higher quality than those fabricated on quartz; resistivities were lower by a factor of 3 and, of greater significance, the temperature coefficient of resistivity was 3.6 times greater. The lower resistivity permits the use of thinner films, and the higher γ improves the temperature sensitivity. Although reasons for the differences were not thoroughly investigated, the larger mismatch in thermal expansion coefficient for the silicide on quartz as compared to silicide on sapphire is one possibility. Inherent differences in NiSi formation on a single crystal Si film vs an evaporated amorphous layer is another possibility.

B. Platinum thermometers

Temperature measurements have also been made using Pt based thermometers. Although the Pt and NiSi thermometers behave similarly, there are several advantages to the Pt films. In particular, Pt, with a melting point of 2045 K, permits measurements without concern for resistivity shifts at the melting transition to substantially higher temperatures than NiSi ($T_{\text{melt}} = 1265$ K).[15] The primary drawback to Pt is the relatively high processing temperatures required to increase the grain size following deposition. This anneal is necessary to yield devices with uniform and reproducible linear resistances in furnace calibrations.

Pt thermometers were fabricated for studies of congruent melting in Si:As alloys.[11] In a single pumpdown, 3 nm Cr, 50 nm Pt, and 3 nm Cr layers were electron beam evaporated onto thermally oxidized silicon wafers. The thin Cr layers were necessary to promote adhesion between the Pt and neighboring layers. The Pt was patterned into 50 μm wide strip line resistors with aspect ratios of 20 using argon ion milling at 500 eV through a 150 nm aluminum mask. The Al mask was used instead of photoresist to avoid photoresist "burn" onto the Pt during milling. Following patterning, the wafers were annealed for 600 °C/120 s and 800 °C/600 s in an AG Associates Heatpulse 410 under flowing Ar. For electrical isolation, an 80 nm silicon nitride layer was grown by PECVD over the Pt thermometers. Nitride proved to be a more robust barrier layer than PECVD oxide; under laser irradiation, PECVD oxide layers typically survived only a single laser pulse before shorting. A Si layer was electron beam deposited on the nitride and then ion implanted with As to the desired concentrations. The Si:As was patterned by reactive ion etching (RIE) with an SF$_6$/O$_2$ plasma, followed by nitride removal with a CHF$_3$/O$_2$ RIE. The Si:As layer, amorphous as formed, was crystallized by a 10 min anneal at 700 °C in flowing Ar. Finally, after a 5 s immersion in a buffered oxide etch, 300 nm aluminum pads were deposited on thermometer contact areas.

Device characterization and calibrations were done following the anneals of the Pt alone, and at the end of device processing. After the first anneals, typical device resistances were 60 Ω ($\rho \approx 15\ \mu\Omega$ cm). Furnace resistance calibrations exhibited a linear temperature dependence to 700 °C, with γ's of 0.0032 K^{-1}. Devices degraded slightly by the end of the processing, primarily during the Si crystallization anneal. Typical device resistances increased to 100 Ω (25 $\mu\Omega$ cm) and γ decreased to 0.0019 K^{-1}.

IV. ANALYSIS OF TEMPERATURE PROFILES

While the temperature measurements at the thermometer layer may provide adequate information for some experiments, in most cases a more thorough analysis of thermometer data is required. With very simple techniques, quantities such as the amount of laser energy stored as heat in the sample can be calculated. With somewhat more effort, analyses relying on numerical heat flow simulations[16] can be used to calculate peak surface temperatures or temperatures at arbitrary depths. In addition, techniques involving heat flow simulations can provide estimates for the absorption coefficient and/or thermal conductivity for poorly characterized layers in the sample structure. In this section, a few of these analysis techniques are elaborated upon.
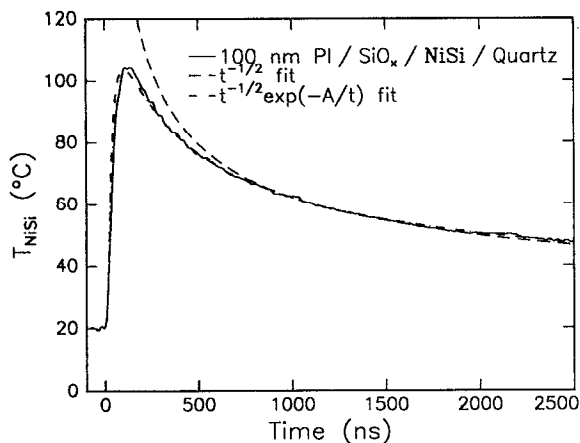
FIG. 4. One and two parameter fits of the NiSi temperature decay for a polyimide film on the NiSi/quartz structure.
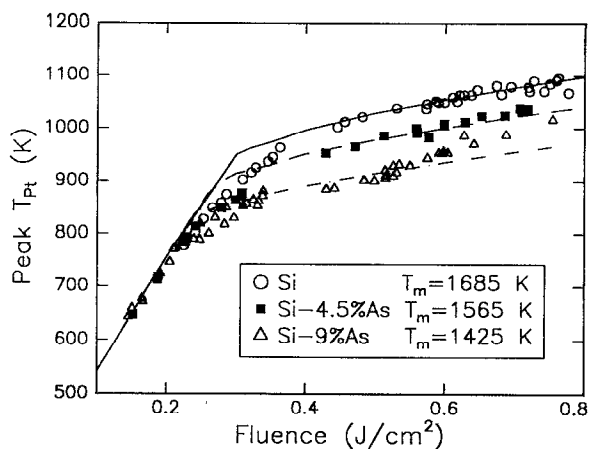

FIG. 5. Fluence dependence of maximum thermometer temperature for pure Si, Si-4.5 at. %As and Si-9 at. %As samples. Lines show heat flow simulations using congruent melting temperatures of 1685 K, 1565 K, and 1425 K, respectively.

A. Retained thermal energy

Energy incident upon a sample may be reflected, consumed in a phase transformation, or retained as heat. This absorbed (retained) heat may be calculated almost directly from the temperature transients using a simple heat flow analysis. The solution to the heat equation[17] for a fluence F deposited instantaneously at the surface of a homogeneous, semi-infinite material at initial temperature T_0 with temperature independent density ρ, specific heat c, thermal conductivity κ, and thermal diffusivity D is given by

$$T(x,t) = T_0 + \frac{F}{\sqrt{\pi \rho c \kappa \, t}} \exp\left(-\frac{x^2}{4Dt} \right). \qquad (4.1)$$

Although the assumptions are not rigorously valid, at long times ($t \gtrsim 1\mu s$) the thermometer becomes nearly isothermal with the surface and does indeed decay as $t^{-1/2}$. This is reasonable since, at long times, heat transport is dominated by the thick substrate and the surface thin films are of little consequence. Fitting the tail of the temperature transient to a $t^{-1/2}$ dependence, coupled with knowledge of the ρ, c, and κ for the substrate, yields the absorbed fluence. Somewhat better fits over a larger time interval can be obtained by treating $x^2/4D$ as a second fitting parameter. Figure 4 illustrates the use of both fits to determine the retained fluence for a KrF laser irradiated polyimide film on NiSi/quartz thermometers. The simple $t^{-1/2}$ fit produces a fluence estimate of 11.4 mJ/cm^2, while adding the second fitting parameter yields 12.0 mJ/cm^2. These values compare well with a measured absorbed fluence of 12.5 mJ/cm^2 ± 10%.

This simple absorbed fluence analysis can provide much useful information. In the laser ablation of polyimide study, this analysis was used to sharply define the ablation threshold fluence, a very critical quantity in characterizing the ablation process.[9] More generally, this analysis provides quantitative data indicating threshold fluences for any irreversible, laser-induced phase transformations involving non-negligible enthalpies of reaction.

B. Congruent melting temperature measurements

The congruent melting temperature of Si:As alloys was also determined using relatively simple analysis of thin film thermometer data. In Fig. 5, the peak temperatures reached by Pt thermometers below various Si:As alloys are plotted as a function of laser fluence. The onset of melting is marked by the change in slope between the low and high fluence regimes. Above some melt threshold energy density, laser energy is primarily absorbed in the enthalpy of melting and the thermometer temperature rises primarily due to motion of the liquid/solid interface toward the thermometer and thermal diffusion. At fluences substantially above the melt threshold, the peak temperature tracks the interface temperature and hence the vertical distance between asymptotic curves is a measure of the melting temperature differences between the alloys (to be precise, for equal interface velocities, the interface temperature difference is measured). Full details can be found in Ref. 11. This analysis, to extract a solid-liquid interface temperature for a solidifying Si:As alloy, can be readily generalized to treat any sample undergoing a laser-induced phase transformation with a planar, moving interface.

C. Heat flow simulations

The thermometer temperature data becomes much more powerful when combined with heat flow simulations of the irradiation process. For well-characterized materials over limited temperature ranges, simulations can, a priori, be very reliable. However, as the accuracy of the input materials parameters decreases, simulations become increasingly unreliable. For these cases, heat flow simulations alone are inadequate and must be combined with other information to obtain reliable temperature information. By simulating laser heating of the entire device structure and comparing simulated and experimental thermometer temperature profiles, one obtains a way to test the plausibility of simulated temperature profiles. Taking this a step further, one can essentially obtain measurements of
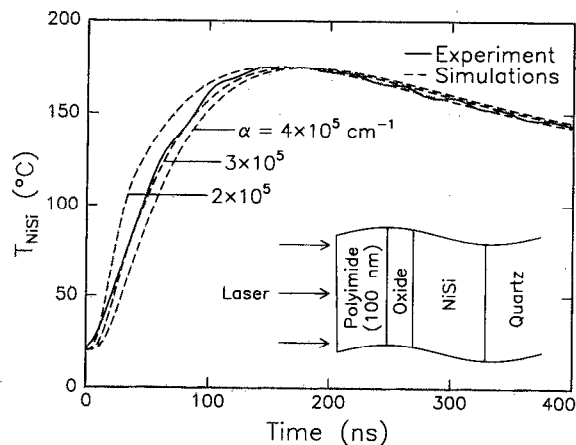
FIG. 6. Effect of absorption coefficient on simulated thermometer profiles for 100 nm polyimide films on NiSi/quartz thermometers.

FIG. 7. Effect of thermal conductivity on laser heating simulations for 200 nm polyimide films on NiSi/quartz thermometers.

poorly known material parameters by adjusting their values until simulated and experimental temperature profiles agree over the entire domain of the temperature transient for many different laser fluences and different surface layer thicknesses. Once values for materials parameters are known, temperatures profiles may be calculated at any depth into the sample structure.

One dimensional heat flow calculations using an explicit finite difference method were used to simulate temperature profiles.[9–11] The simulations modeled the full device structure including temperature dependent materials parameters (e.g., specific heat, thermal conductivity, and absorption coefficient) and assumed Beer's law for absorption of the laser radiation. Variable layer thicknesses and time steps were used with fine layers near the surface, where temperature gradients were large, and thick layers in the bulk.

For samples with strongly absorbing and well-characterized surface layers, numerical modeling, constrained by direct temperature measurements, can be used to eliminate small uncertainties in simulation assumptions. The determination of Si:As congruent melting temperatures provides an example of this mode. Simulations with control samples (0% As) provided Si_3N_4 thermal conductivity measurements necessary for the congruent melting temperature calculations.[11] For samples with moderately absorbing and/or poorly characterized surface layers, numerical modeling of temperature profiles requires considerably more effort. The polyimide on NiSi thermometers study provides a good example.[9] In the discussion that follows, the role the absorption coefficient, α, and thermal conductivity play in simulation profiles is illustrated.

The effect of the absorption coefficient upon simulated thermometer temperature profiles is most pronounced early in the thermometer transient and for thin surface layers. Energy deposition into the sample is determined by α according to Beer's law. A large α implies most of the energy is absorbed near the surface and hence heat must be transported essentially through the entire thickness of the surface layer before heating the thermometer. This results
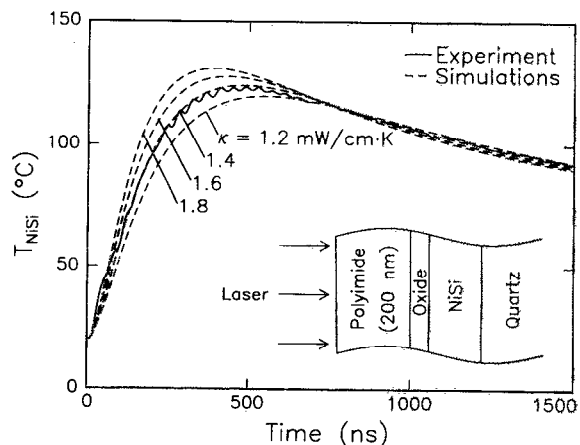
in slower thermometer heating than would occur if α were smaller. For low values of α, a fair fraction of the deposited energy occurs close to the thermometer. As shown in Fig. 6, the simulated NiSi temperature increases less rapidly as α is increased from 2 to 4×10^5 cm^{-1} for a 100 nm polyimide layer on the NiSi/quartz structure. The fluence, constant in these simulations, was chosen to match the long time behavior of the temperature transient.

The thermal conductivity of the absorbing film plays an important role in the thermometer temperature profile for early and intermediate times. Laser energy is deposited nonuniformly into the sample and, for a given heat capacity, the thermal conductivity governs the resulting heat flow. Large values for κ result in heating of the thermometer to higher temperatures and at faster rates. This can be seen in the simulations of Fig. 7. A higher NiSi temperature occurs at an earlier time as the polyimide thermal conductivity is increased from 1.2 to 1.8×10^{-3} W/cm K.

The fact that the absorption coefficient and thermal conductivity play important roles in thermometer temperature profiles in somewhat different regimes allows one to match simulated and experimental temperature profiles in a systematic fashion, with literature values of materials properties used as an initial guide. However, it is important to note that for very strong absorbers (or good conductors), the indicated sensitivity to changes in values may not occur because a regime of essentially pure surface absorption (or thermal shorting) may be achieved.

ACKNOWLEDGMENTS

[1] See, for example, proceedings of conferences in Mater. Res. Soc. Symp. Proc. **100** (1988); **157** (1989); **205** (1992); **235** (1992); and **285** (1993).

[2] B. C. Larson, C. W. White, T. S. Noggle, and D. Mills, Phys. Rev. Lett. **48**, 337 (1982).

[3] A. Compaan, Mater. Res. Soc. Symp. Proc. **35**, 65 (1985).

[4] H. K. Park, X. Xu, C. P. Grigoropoulos, N. Do, L. Klees, P. T. Leung, and A. C. Tam, Appl. Phys. Lett. **61**, 749 (1992).

[5] J. W. Herman and H. E. Elsayed-Ali, Phys. Rev. Lett. **69**, 1228 (1992).

[6] I.-Y. Sandy Lee, X. Wen, W. A. Tolbert, D. D. Dlott, M. Doxtader, and D. R. Arnold, J. Appl. Phys. **72**, 2440 (1992).

[7] M. O. Thompson, Mater. Res. Soc. Symp. Proc. **100**, 525 (1988).

[8] T. Sameshima, M. Hara, and S. Usui, Jpn. J. Appl. Phys. **28**, L2131 (1989).

[9] D. P. Brunco, M. O. Thompson, C. E. Otis, and P. M. Goodwin, J. Appl. Phys. **72**, 4344 (1992).

[10] D. P. Brunco, M. O. Thompson, C. E. Otis, and P. M. Goodwin, Mater. Res. Soc. Symp. Proc. **285** (1993) (in press).

[11] J. A. Kittl, R. Reitano, M. J. Aziz, D. P. Brunco, and M. O. Thompson, J. Appl. Phys. **73**, 3725 (1993).

[12] M. O. Thompson, Ph.D. thesis, Cornell University, 1984.

[13] S. P. Kowalczyk, C. D. Dimitrakopoulos, and S. E. Molis, Mater. Res. Soc. Symp. Proc. **227**, 55 (1991).

[14] Nichrome etchant was used because it was immediately available, wet nickel etchants are also sold by Transene.

[15] M. Hansen, *Constitution of Binary Alloys*, 2nd ed. (McGraw-Hill, New York, 1958).

[16] P. Baeri and S. U. Campisano, *Laser Annealing of Semiconductors*, edited by J. M. Poate and J. W. Mayer (Academic, New York, 1982), p. 75.

[17] H. S. Carslaw and J. C. Jaeger, *Conduction of Heat in Solids*, 2nd ed. (Clarendon, Oxford, 1959).